Shinotsuka *et al. EURASIP Journal on Advances in Signal Processing* (2015) 2015:82
DOI 10.1186/s13634-015-0266-2

EURASIP Journal on Advances in Signal Processing
a SpringerOpen Journal

RESEARCH Open Access

# Analyzing radio interferometric positioning systems with undersampling receivers

Marie Shinotsuka[1*], Yiyin Wang[2], Xiaoli Ma[1] and G. Tong Zhou[1]

**Abstract**

Radio interferometric positioning systems are developed for localization in wireless sensor networks (WSNs), and they have the potential to yield highly accurate location information at low computational cost and implementation complexity. In the radio interferometric positioning system (RIPS), two transmitters transmit sinusoidal signals at slightly different frequencies, and two receivers pass the received signals through square-law devices to produce low-frequency differential signals. However, a squaring operation increases the noise power, leading to performance loss. To avoid this problem, a receiver for the RIPS using undersampling techniques (RIPS-u) has been proposed. In this paper, we investigate the performance of the RIPS with a square-law device (RIPS-sq) and the performance of the RIPS-u through theoretical and experimental analyses. Specifically, we compute Cramér-Rao lower bounds (CRLBs) of the range and location estimates in both systems and show that the RIPS-u has lower CRLBs than the RIPS-sq. Furthermore, we have carried out experimental tests by implementing both systems on National Instruments (NI) Universal Software Radio Peripherals (USRPs). From both the theoretical and experimental results, the effectiveness of the RIPS-u over the RIPS-sq is confirmed.

**Keywords:** Wireless sensor network; Localization; Radio interferometric positioning system

## 1 Introduction

Advances in technology have enabled small-sized devices equipped with sensors to form wireless sensor networks (WSNs) [1]. These small devices act as nodes in WSNs, and their location information is a critical part of the sensor data [2]. Thus, localization has to be performed when node locations are unknown [3]. Global Positioning System (GPS) is a well-known example for localization. The global coverage and wide availability in commercial devices make GPS attractive. However, GPS requires a line-of-sight (LOS) path from the satellites in order to function, and this renders GPS inadequate for indoor scenarios. Furthermore, power consumption and computational costs of GPS are often prohibitively high for resource-limited WSNs [4]. For the same reason, ultra-wideband (UWB)-based localization systems, which are known for high accuracy and robustness to multipath [5, 6], are also considered as unsuitable for WSNs [4]. Hence, the investigation of highly accurate localization systems using narrowband signals with low complexity is of great interest. One such system is the radio interferometric positioning system (RIPS) [7].

The RIPS is categorized as a range-based system, where the location is estimated from range measurements. The RIPS model to obtain range information is illustrated in Fig. 1. Each ranging session involves four nodes (two transmitters and two receivers); two transmitter nodes transmit pure sinusoidal signals at slightly different frequencies to produce slowly varying envelopes at the receivers. The range information is contained in the phases of the received signals, and the difference of the phases at two receivers yields a range metric called Q-range $q = d_{1,1} - d_{1,2} - d_{2,1} + d_{2,2}$, where $d_{k,m}$ is the distance between the $k$th transmitter and the $m$th receiver; (see Fig. 1 for illustration). After obtaining multiple Q-range measurements, node locations can be estimated. In [7, 8], several iterative approaches with genetic algorithm are used to collectively estimate the node locations in WSNs. Since iterative approach is computationally demanding, the computation is done at a centralized server. Another approach is a hyperbolic positioning method [9], which locates a single node at a time. In this

*Correspondence: gtg594x@mail.gatech.edu
[1] School of Electrical and Computer Engineering, Georgia Institute of Technology, 30332-0250 Atlanta, GA, USA
Full list of author information is available at the end of the article

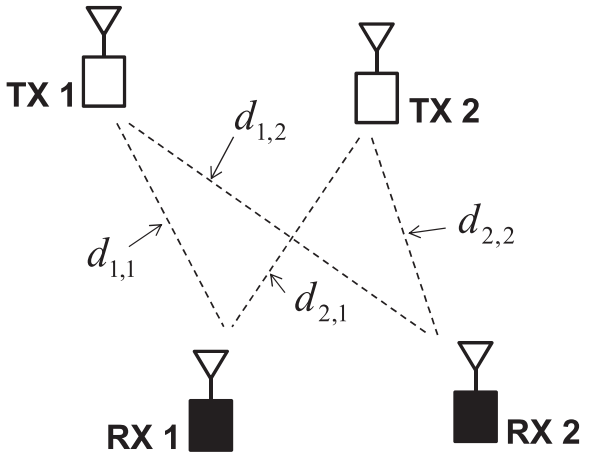


**Fig. 1** The radio interferometric ranging technique

paper, we show that the Q-range can be converted to the range difference (RD), and the location can be estimated linearly when enough Q-range measurements are available.

In the original RIPS in [7], each receiver is equipped with a square-law device to extract a low-frequency differential signal. However, squaring the signal increases the noise power, which in turn deteriorates the range-estimation performance. To avoid this problem, the RIPS with receivers using undersampling techniques (RIPS-u) is proposed in [10]. The transmitter model of the RIPS-u is the same as the original RIPS with a square-law device (RIPS-sq), but the RIPS-u directly samples the signal without squaring operation. While the complexity of the RIPS-u is reduced from that of the RIPS-sq by removing the square-law device, the results presented in [10] show that the RIPS-u yields a 3-dB performance gain over the RIPS-sq, and thus the RIPS-u holds great promise.

In this paper, we investigate the performance of the RIPS-u and the RIPS-sq through theoretical and experimental analyses to confirm that the RIPS-u has better performance than the RIPS-sq. For the theoretical analysis, we compute Cramér-Rao lower bounds (CRLBs) for the Q-range and location estimates in both systems. We show that with least-squares (LS) estimators, the resulting performances approach the CRLBs. We have also implemented both systems using National Instruments (NI) Universal Software Radio Peripherals (USRPs) and further confirm the efficiency of the RIPS-u over the RIPS-sq.

The rest of this paper is organized as follows. An overview of the RIPS and related work are briefly discussed in Section 2. In Section 3, the system models of the RIPS-u and the RIPS-sq are described. Their performances are analyzed theoretically by investigating the CRLBs of the Q-range estimates and the location estimates in Section 4. Simulation results are shown in Section 5, and experimental results are presented in Section 6. Finally, conclusions are drawn in Section 7.

### 1.1 Notations

Bold uppercase letters denote matrices. Bold lowercase letters denote vectors. $\mathcal{CN}(\mu, \sigma^2)$ refers to a complex Gaussian distribution with mean $\mu$ and variance $\sigma^2$, and $\mathcal{U}(a, b)$ signifies a uniform distribution over the range $[a, b]$. Superscripts $(\cdot)^{\mathrm{T}}$, $(\cdot)^{\mathrm{H}}$, $(\cdot)^*$, and $(\cdot)^\dagger$ denote transpose, Hermitian transpose, complex conjugate, and pseudo-inverse, respectively.

## 2 Related work

Because of its flexibility and low complexity, the RIPS has been applied for various scenarios. One of which is to track mobile nodes [11–13]. In [11], a mobile node tracking system based on the RIPS called inTrack is proposed to analyze the effects of velocity and moderate outdoor multipath on the system performance. The system is further improved in [12] by incorporating a Doppler shift into location estimation. Their experimental results show a mean absolute error (MAE) of 37 cm. Also taking a Doppler shift into account and using an extended Kalman filter, a tracking system based on the RIPS yields the MAE of 1.68 m in a field test [13]. Another extension of the RIPS is its implementation at a different frequency band. Formerly, the RIPS is implemented on CC1000 RF transceiver [14] at the frequency band below 1 GHz. However, in [15, 16], the RIPS is implemented on CC2430 transceivers [17], which operate at 2.4 GHz. Due to lack of fine-frequency tuning capability of the CC2430 platform, an inherent offset of local oscillators is used for the frequency difference, resulting in the MAE of 1.5–2 m [15]. Using the same platform, a stochastic RIPS (SRIPS) [16] is proposed to improve the accuracy at 2.4 GHz by taking into account some stochastic properties of Q-range measurements.

To use the RIPS for multipath-rich indoor environments, a multihop scheme is proposed in [18]. The approach is similar to [19], where sinusoids are transmitted at multiple frequencies, and a subspace-based method is used to detect the first-arriving path. On the other hand, the ranging signal of the RIPS is modified in [20–22] to make the system robust to the fading. A dual-tone RIPS (DRIPS) [20] uses dual-tone signaling to cancel the phase shifts due to fading. Synchronized anchor nodes transmit dual-tone signals simultaneously, which allow the target node to directly estimate its position. The DRIPS is further enhanced in uDRIPS [21] by employing undersampling techniques at the receiver. A space-time RIPS (STRIPS) [22] uses a space-time code and millimeter wave (MMW) band to combat fading and multipath effects. These aforementioned are some of the examples, and they show the flexibility of the RIPS. However, to the best of our knowledge, formal investigation of the performance

bounds for the RIPS has not appeared in the literature. Our theoretical analysis presented in this paper can serve as benchmark to gauge various proposed algorithms.

## 3 System model

### 3.1 Transmitter design

A typical RIPS consists of two transmitters and two receivers in each ranging session. These nodes require perfect frequency synchronization. Time synchronization is required between two receivers, but the transmitters can be asynchronous. The transmitted signal at the $k$th transmitter node in a band-pass complex form is represented as

$$s_k(t) = a_k e^{j\theta_k} e^{j2\pi f_k t},\ k = 1, 2, \tag{1}$$

where $a_k e^{j\theta_k}$ and $f_k$ are the complex amplitude and the frequency, respectively, of the signal transmitted by the $k$th node. Let us further define $\Delta = f_1 - f_2$ and $g = (f_1 + f_2)/2$. We assume $f_1 > f_2$ without loss of generality.

The block diagram of the RIPS-u and the RIPS-sq is shown in Fig. 2. The received signal at the $m$th receiver is modeled as

$$r_m(t) = a_1 e^{j2\pi(f_1 - f_o)t} e^{-j\varphi_{1,m}} + a_2 e^{j2\pi(f_2 - f_o)t} e^{-j\varphi_{2,m}} + \nu_m(t),\quad m = 1, 2, \tag{2}$$

where $f_o$ is the frequency of the local oscillator that down-converts the signal to an intermediate frequency band, $\varphi_{k,m} = 2\pi f_k \left(d_{k,m}/c + t_k\right) - \theta_k$ is the phase of the received signal from the $k$th transmitter to the $m$th receiver, $d_{k,m}$ is the distance between the $k$th transmitter and the $m$th receiver, $c$ denotes the speed of light ($c = 3 \times 10^8$ m/s), $t_k$ is the unknown time instant when the $k$th node starts its transmission, and $\nu_m(t)$ is the additive noise. Although the RIPS works in the presence of stationary noise in general, for purposes of finding the CRLBs, we assume $\nu_m(t)$ to be white Gaussian noise denoted as $\nu_m(t) \sim \mathcal{CN}\left(0, \sigma_m^2\right)$ in this paper. In other words, the real and imaginary parts of $\nu_m(t)$ are assumed to be mutually independent real-valued white Gaussian processes with zero mean and variance $\sigma_m^2/2$.

### 3.2 Receiver design in the RIPS-sq

In the RIPS-sq [7], the received signal $r_m(t)$ is passed through a band-pass filter (BPF) to remove the out-of-band noise. Then, a square-law device squares the output of the BPF, and a low-pass filter (LPF) removes high-frequency components beyond $\Delta$. The output of the LPF is a low-frequency differential signal $\widetilde{r}_m(t)$, which only contains the frequency components at $\pm\Delta$. Sampling $\widetilde{r}_m(t)$ at the rate $f_s \geq 2\Delta$, we obtain

$$\widetilde{r}_m[n] = a_1 a_2 e^{j2\pi\Delta n/f_s - j\phi_m} + a_1 a_2 e^{-j2\pi\Delta n/f_s + j\phi_m} + \widetilde{\nu}_m[n], \tag{3}$$

where $\phi_m = \varphi_{1,m} - \varphi_{2,m} = 2\pi f_1(d_{1,m}/c + t_1) - \theta_1 - 2\pi f_2(d_{2,m}/c + t_2) + \theta_2$, and $\widetilde{\nu}_m[n]$ is the sampled aggregated noise, which includes a noise product term and signal-noise product terms. Mathematically, $\widetilde{\nu}_m[n]$ can be written as

$$\widetilde{\nu}_m[n] = \nu_m^*[n] \sum_{k=1}^{2} a_k e^{j2\pi(f_k - f_o)n/f_s - j\varphi_{k,m}} + \nu_m[n] \sum_{k=1}^{2} a_k e^{-j2\pi(f_k - f_o)n/f_s + j\varphi_{k,m}} + \nu_m[n]\,\nu_m^*[n]. \tag{4}$$

Statistics of $\widetilde{\nu}_m[n]$ are investigated in Section 4.1. Collecting $N$ samples and stacking them vertically, (3) can be represented in a matrix-vector form as

$$\widetilde{\mathbf{r}}_m = \widetilde{\mathbf{H}}\widetilde{\mathbf{z}}_m + \widetilde{\mathbf{v}}_m, \tag{5}$$

where $\widetilde{\mathbf{r}}_m$ and $\widetilde{\mathbf{v}}_m$ are column vectors of samples from $\widetilde{r}_m(t)$ and $\widetilde{\nu}_m(t)$, respectively, $\widetilde{\mathbf{H}} = \left[\mathbf{h}\left(\Delta, f_s\right), \mathbf{h}\left(-\Delta, f_s\right)\right]$, $\mathbf{h}\left(f, f_s\right) = \left[1, e^{j2\pi f/f_s}, \ldots, e^{j2\pi(N-1)f/f_s}\right]^T$, and $\widetilde{\mathbf{z}}_m = \left[a_1 a_2 e^{-j\phi_m}, a_1 a_2 e^{j\phi_m}\right]^T$.

Notice that the range information is in the phase of $\widetilde{\mathbf{z}}_m$. To estimate the Q-range, the following assumptions are

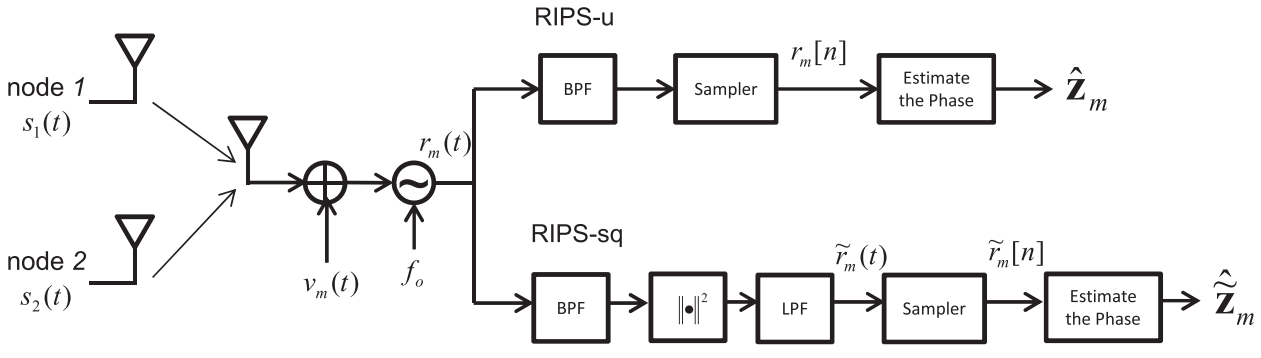


**Fig. 2** The block diagram of RIPS-u and RIPS-sq

made [7]: (1) $\Delta \ll g$, i.e., $f_1 - f_2 \ll (f_1 + f_2)/2$; (2) $|q| < c/2g$, where $q = d_{1,1} - d_{1,2} - d_{2,1} + d_{2,2}$ is the Q-range. From these assumptions, the phase difference at two receivers can be approximated as [7]

$$\frac{c}{2\pi g}(\phi_1 - \phi_2) = q + \eta \approx q, \tag{6}$$

where $\eta = \frac{\Delta}{4\pi g}\left(d_{1,1} - d_{1,2} + d_{2,1} - d_{2,2}\right)$. Hence, the Q-range is estimated in the RIPS-sq as [7]

$$\widehat{q}^{(\mathrm{sq})} = \frac{c}{2\pi g}\left(\widehat{\phi}_1 - \widehat{\phi}_2\right), \tag{7}$$

where $\widehat{\phi}_m$ is the estimated phase at the $m$th receiver. One way to estimate the phase is by using an LS estimator. Assuming the frequencies are known at the receivers, $\phi_m$ can be estimated as

$$\widehat{\phi}_m = \arg\left(\left[\widehat{\mathbf{z}}_m\right]_1^* + \left[\widehat{\mathbf{z}}_m\right]_2\right), \tag{8}$$

where $\widehat{\mathbf{z}}_m = \widetilde{\mathbf{H}}^{\dagger}\widetilde{\mathbf{r}}_m$ and $[\mathbf{z}]_i$ denotes the $i$th element of the vector $\mathbf{z}$.

From (6), it is apparent that as $\Delta$ increases, $\eta$ becomes a dominant source of error in the range estimation of the RIPS-sq. Moreover, since the range is estimated from the phase, an unknown integer is present when $|q| > c/2g$, which results in integer ambiguity. In this paper, we call the maximum range that causes no integer ambiguity as a *resolvable range*. Here, the resolvable range in the RIPS-sq is $c/2g$.

In practice, the Q-range is likely to be larger than the resolvable range, and multiple Q-range measurements at different frequencies are obtained to resolve the integer ambiguity [7]. The unknown integers can be calculated with the maximum likelihood estimator (MLE) [23], the Chinese remainder theorem (CRT) [24, 25], or lattice reduction method [26]. In this paper, we ignore the integer ambiguity for simplicity and choose the parameters for simulations and experiments to avoid ambiguous measurements.

### 3.3 Receiver design in the RIPS-u

In the RIPS-u [10], the received signal $r_m(t)$ in (2) is passed through a BPF and directly sampled at the rate $f_u$, i.e.,

$$\begin{aligned} r_m[n] = {} & a_1 e^{j2\pi(f_1 - f_o)n/f_u} e^{-j\varphi_{1,m}} + a_2 e^{j2\pi(f_2 - f_o)n/f_u} e^{-j\varphi_{2,m}} \\ & + v_m[n]. \end{aligned} \tag{9}$$

The receiver design of the RIPS-u is illustrated in the upper half of Fig. 2. At the $m$th receiver, $N$ samples are collected, which are modeled as

$$\mathbf{r}_m = \mathbf{H}\mathbf{z}_m + \mathbf{v}_m, \tag{10}$$

where $\mathbf{r}_m$ and $\mathbf{v}_m$ are the sampled vectors of $r_m[n]$ and $v_m[n]$, respectively, $\mathbf{H} = \left[\mathbf{h}\left(f_1 - f_o, f_u\right)\ \mathbf{h}\left(f_2 - f_o, f_u\right)\right]$, and $\mathbf{z}_m = \left[a_1 e^{-j\varphi_{1,m}},\ a_2 e^{-j\varphi_{2,m}}\right]^T$. As shown in [10], even $f_u < 2\left(f_k - f_o\right)$, where the frequencies are aliased, the RIPS-u can still accurately estimate the phase as long as the aliased frequencies are well separated. In other words, the frequencies are to be designed to satisfy the condition such that $\mod(\Delta, f_u) \neq 0$ to prevent frequencies from aliasing onto each other, where $\mod(\Delta, f) = \Delta - f\lfloor \Delta/f \rfloor$ with $\lfloor\cdot\rfloor$ denoting the floor function.

Assuming the knowledge of designed parameters is shared among all the participating nodes, the LS estimator for the phase vector $\mathbf{z}_m$ is

$$\widehat{\mathbf{z}}_m = \mathbf{H}^{\dagger}\mathbf{r}_m. \tag{11}$$

When $|d_{1,1} - d_{1,2}| < c/(2f_1)$ and $|d_{2,1} - d_{2,2}| < c/(2f_2)$, no unknown integers are generated from phase unwrapping. In such a case, a Q-range estimator of the RIPS-u is given as

$$\begin{aligned} \widehat{q}^{(u)} = {} & \frac{c}{2\pi}\left\{\frac{1}{f_1}\arg\left([\widehat{\mathbf{z}}_1]_1^*\,[\widehat{\mathbf{z}}_2]_1\right) + \frac{1}{f_2}\arg\left([\widehat{\mathbf{z}}_1]_2\,[\widehat{\mathbf{z}}_2]_2^*\right)\right\} \\ = {} & \frac{c}{2\pi}\left(\frac{\widehat{\varphi}_{1,1} - \widehat{\varphi}_{1,2}}{f_1} - \frac{\widehat{\varphi}_{2,1} - \widehat{\varphi}_{2,2}}{f_2}\right). \end{aligned} \tag{12}$$

Notice that the formation of the estimator in (12) does not involve any approximation in contrast to (7) for the RIPS-sq. Moreover, the RIPS-sq requires the frequencies to satisfy $\Delta \ll f_1, f_2$ to attain a small approximation error and to guarantee a slowly varying envelope of the received signal. Such a requirement is not imposed in the RIPS-u, and thus, the RIPS-u has wider applicability.

Unfortunately, neither the RIPS-u nor the RIPS-sq is robust to multipath [27]. This is because the fading channel causes unknown phase shifts in the received signal. As four nodes are spatially apart, four links in Fig. 1 have independent channels. Hence, the phase shifts due to multipath fading cannot be canceled out with the Q-range estimators of both systems, resulting in the biased Q-range estimates. To effectively combat the multipath fading effects, the methods [20–22] discussed in Section 2 should be considered.

### 3.4 Localization

In the original RIPS [7], locations of the nodes in the WSN are estimated collectively. The iterative algorithm used in [7] is computationally expensive, and a dedicated server is required to perform the localization. However, by restricting the Q-range measurements to have one unknown node, localization can be performed at lower complexity. The assumption we made here is applicable when we have enough anchor nodes and one target node or localizing one node at a time [12].

When there exists only one node with unknown position in a ranging session, the Q-range can be converted

to the range difference (RD). For example in Fig. 1, let us assume that TX2, RX1, and RX2 are at known positions, and TX1 is the target node to be localized. Then, the last two terms in the Q-range $q = d_{1,1} - d_{1,2} - d_{2,1} + d_{2,2}$ can be pre-calculated. Moving the unknown terms to the left-hand side (LHS), we arrive at the RD measurement between TX1 and two receivers as

$$d_{1,1} - d_{1,2} = q + d_{2,1} - d_{2,2}. \tag{13}$$

Let us denote the coordinates of the target node and the $m$th receiver as $\mathbf{x}$ and $\mathbf{x}_m$, respectively. Choosing the first receiver node as the origin of the coordinate system ($\mathbf{x}_1 = \mathbf{0}$), (13) can be rewritten as

$$\|\mathbf{x}\| - \|\mathbf{x} - \mathbf{x}_2\| = R, \tag{14}$$

where $R$ is the right-hand side (RHS) of (13) and $\|\mathbf{x}\|$ denotes the Euclidean norm of the vector $\mathbf{x}$. Rearranging the terms and squaring both sides as

$$\|\mathbf{x} - \mathbf{x}_2\|^2 = (\|\mathbf{x}\| - R)^2, \tag{15}$$

we arrive at

$$2R\|\mathbf{x}\| - 2\mathbf{x}_2^T\mathbf{x} = R^2 - \|\mathbf{x}_2\|^2, \tag{16}$$

where the unknown terms are collected on the LHS, and the known terms are on the RHS. When we consider a 2D scenario, the dimension of $\mathbf{x}$ is 2. Keeping $\mathbf{x}_1$ fixed as the reference node over multiple RD measurements, we have $\mathbf{x}$ and $\|\mathbf{x}\|$ as unknowns. Hence, with at least three independent RD measurements, we have a set of linear equations to solve the location vector $\mathbf{x}$. Details of RD-based localization algorithms with linear estimators can be found in [28, 29].

## 4 Performance analysis

In this section, we derive the CRLB for both the RIPS-u and the RIPS-sq based on the system models described in Section 3. We first compute the CRLBs of $\phi_m$ and $\varphi_{k,m}$ for the RIPS-sq and the RIPS-u, respectively, and perform the vector transformation to achieve the CRLBs of the Q-range estimates. In the following analysis, we assume that the Q-range is within the resolvable range for both systems, and thus we do not consider the integer ambiguity issue.

### 4.1 The CRLB of the Q-range estimate in the RIPS-sq

To derive the CRLB in the RIPS-sq, the statistical properties of the aggregated noise $\widetilde{\nu}_m[n]$ are analyzed first. Since $\nu_1[n]$ and $\nu_2[n]$ at a given time instant $n$ are treated as mutually independent Gaussian random variables ($\nu_m[n] \sim \mathcal{CN}(0, \sigma_m^2)$) and the signal is squared at each receiver independently, the aggregated noise at each receiver $\widetilde{\nu}_1[n]$ and $\widetilde{\nu}_2[n]$ are also mutually independent. Thus, the first- and second-order statistics of $\widetilde{\nu}_m[n]$ are given as [10]

$$E[\widetilde{\nu}_m[n]] = \sigma_m^2, \tag{17}$$

$$\mathrm{var}[\widetilde{\nu}_m[n]] = \sigma_m^4 + 2\sigma_m^2\|u_m[n]\|^2, \tag{18}$$

$$\widetilde{\sigma}_m^2[n] \triangleq \mathrm{var}[\widetilde{\nu}_m[n]], \tag{19}$$

where $u_m[n] = \sum_{k=1}^{2} a_k e^{j2\pi(f_k - f_o)n/f_s} e^{-j\varphi_{k,m}}$ and recall $\varphi_{k,m} = 2\pi f_k\left(d_{k,m}/c + t_k\right) - \theta_k$. Notice that the noise variance depends on $n$. Hence, let us further approximate $\widetilde{\sigma}_m[n]$ by its mean over the random parameter $\theta_k \sim \mathcal{U}(-\pi/2, \pi/2)$ in $\varphi_{k,m}$ as

$$\bar{\sigma}_m^2 = E_{\theta_k}\left[\widetilde{\sigma}_m^2[n]\right] = \sigma_m^4 + 2\sigma_m^2\left(a_1^2 + a_2^2\right). \tag{20}$$

The exact distribution of the aggregated noise is difficult to derive. Instead, we use the approximation in (20) and model the aggregated noise as a normally distributed random variable such that $\widetilde{\nu}_m[n] \sim \mathcal{N}\left(\sigma_m^2, \bar{\sigma}_m^2\right)$. Later in this paper, we show that the Monte Carlo simulation results match well with the CRLB derived based on the Gaussian approximation, and thus the Gaussian approximation yields meaningful results.

The interest here is to find the CRLB of $\phi_m$. The low-frequency differential signal in (3) can be equivalently written as a real sinusoid with an additive noise as

$$\widetilde{r}_m[n] = 2a_1a_2\cos\left(\frac{2\pi\Delta n}{f_s} - \phi_m\right) + \widetilde{\nu}_m[n]. \tag{21}$$

Since we model $\widetilde{\nu}_m[n]$ as Gaussian, the log-likelihood function for $\widetilde{\mathbf{r}}_m$ is represented as

$$\ln p(\widetilde{\mathbf{r}}_m; \phi_m) = -\frac{N}{2}\ln\left(2\pi\bar{\sigma}_m^2\right) - \frac{1}{2\bar{\sigma}_m^2}\sum_{n=0}^{N-1}\left(\widetilde{r}_m[n] - 2a_1a_2\cos\left(\frac{2\pi\Delta n}{f_s} - \phi_m\right) - \sigma_m^2\right)^2. \tag{22}$$

Taking a second derivative of (22) w.r.t. $\phi_m$, we obtain

$$\frac{\partial^2 \ln p(\widetilde{\mathbf{r}}_m; \phi_m)}{\partial\phi_m^2} = -\left(\frac{2a_1a_2}{\bar{\sigma}_m}\right)^2\sum_{n=0}^{N-1}\left\{\sin^2\left(\frac{2\pi\Delta n}{f_s} - \phi_m\right) - \cos^2\left(\frac{2\pi\Delta n}{f_s} - \phi_m\right) + \frac{1}{2a_1a_2}\widetilde{r}_m[n]\cos\left(\frac{2\pi\Delta n}{f_s} - \phi_m\right) - \frac{\sigma_m^2}{2a_1a_2}\cos\left(\frac{2\pi\Delta n}{f_s} - \phi_m\right)\right\}. \tag{23}$$

To compute the CRLB of $\phi_m$, we need to take the expectation of (23). Notice that $E[\widetilde{r}_m[n]] = 2a_1a_2\cos\left(\frac{2\pi\Delta n}{f_s} - \phi_m\right) + \sigma_m^2$, where the second term is due to the non-zero mean of $\widetilde{\nu}_m[n]$ as shown in (19).

Hence, using the trigonometric identities, the CRLB of $\phi_m$ becomes

$$\begin{aligned}\mathrm{CRLB}(\phi_m) &= -\left(E\left[\frac{\partial^2 \ln p(\tilde{\mathbf{r}}_m;\phi_m)}{\partial \phi_m^2}\right]\right)^{-1} \\ &= 2\left(\frac{\bar{\sigma}_m}{2a_1a_2}\right)^2\left\{N-\sum_{n=0}^{N-1}\cos\left(\frac{4\pi\Delta n}{f_s}-2\phi_m\right)\right\}^{-1}.\end{aligned} \tag{24}$$

Recall that in the RIPS-sq, the signal is sampled at the rate $f_s > 2\Delta$. Hence, we assume that $\mod(2\Delta, f_s)$ is not near 0 or 0.5, which yields the approximations $\sum_{n=0}^{N-1}\cos\left(\frac{4\pi\Delta n}{f_s}-2\phi_m\right)\approx 0$ ([30] pp. 56), and the CRLB in (24) becomes

$$\mathrm{CRLB}(\phi_m) \approx \frac{2}{N}\left(\frac{\bar{\sigma}_m}{2a_1a_2}\right)^2. \tag{25}$$

From (7), in the RIPS-sq, the Q-range is approximated as $\widehat{q}^{(\mathrm{sq})} \approx \frac{c}{2\pi g}\left(\widehat{\phi}_1-\widehat{\phi}_2\right)$ given $\Delta \ll g$. By performing the vector transformation, the CRLB of the Q-range estimate in the RIPS-sq is calculated as

$$\begin{aligned}\mathrm{CRLB}\left(q^{(\mathrm{sq})}\right) &= \left(\frac{c}{2\pi g}\right)^2\left(\mathrm{CRLB}(\phi_1)+\mathrm{CRLB}(\phi_2)\right) \\ &= \left(\frac{c}{2\pi}\right)^2\frac{\bar{\sigma}_1^2+\bar{\sigma}_2^2}{2N}\left(\frac{1}{a_1a_2g}\right)^2.\end{aligned} \tag{26}$$

Notice that the CRLB depends on $\bar{\sigma}_m^2$, $a_k$, $g$, and $N$. According to (26), the CRLB decreases as the noise variance $\bar{\sigma}_m^2$ decreases, and $N$ and $g$ increase. Note, however, when transmitters transmit with high frequencies, the resolvable range becomes small, and the Q-range estimates are likely to experience the integer ambiguity problem.

### 4.2 The CRLB of the Q-range estimate in the RIPS-u

The CRLB of the Q-range estimate in the RIPS-u is derived based on the system model in (10). Since the noise variance is independent of the parameter $\varphi_{k,m}$, the Fisher information matrix (FIM) $\mathbf{J}$ for the parameter vector $\boldsymbol{\varphi}_m = [\varphi_{1,m}, \varphi_{2,m}]^T$ under the complex Gaussian noise is expressed as ([30] pp. 525)

$$\left[\mathbf{J}(\boldsymbol{\varphi}_m)\right]_{kl} = \frac{1}{\sigma_m^2}\dot{\mathbf{h}}(\varphi_{k,m})^{\mathrm{H}}\dot{\mathbf{h}}(\varphi_{l,m}), \tag{27}$$

where $[\mathbf{J}]_{kl}$ denotes the element in the matrix $\mathbf{J}$ at the $k$th row and the $l$th column and

$$\dot{\mathbf{h}}(\varphi_{k,m}) = \begin{bmatrix}\mathbf{h}\left(f_k-f_o,f_u\right)(-j)a_k e^{-j\varphi_{k,m}} \\ \mathbf{h}^*\left(f_k-f_o,f_u\right)ja_k e^{j\varphi_{k,m}}\end{bmatrix}. \tag{28}$$

Substituting (28) into (27), we arrive at

$$\mathbf{J}(\boldsymbol{\varphi}_m) = 2\left(\frac{1}{\sigma_m}\right)^2\begin{bmatrix}a_1^2N & a_1a_2\sum_{n=0}^{N-1}\cos\left(\frac{2\pi\Delta n}{f_u}-\phi_m\right) \\ a_1a_2\sum_{n=0}^{N-1}\cos\left(\frac{2\pi\Delta n}{f_u}-\phi_m\right) & a_2^2N\end{bmatrix}. \tag{29}$$

Taking the inverse of $\mathbf{J}(\boldsymbol{\varphi}_m)$, the CRLB of $\varphi_{k,m}$ is achieved along the diagonal as

$$\mathrm{CRLB}(\varphi_{k,m}) = \frac{N}{2}\left(\frac{\sigma_m}{a_k}\right)^2\left\{N^2-\left(\sum_{n=0}^{N-1}\cos\left(\frac{2\pi\Delta n}{f_u}-\phi_m\right)\right)^2\right\}^{-1}. \tag{30}$$

Recall that to avoid closely aliased frequencies, the parameters are chosen so that $\mod(\Delta, f_u) \neq 0$. Therefore, similarly to the approximation that we made in the RIPS-sq, we assume that $\sum_{n=0}^{N-1}\cos\left(\frac{2\pi\Delta n}{f_u}-\phi_m\right) \approx 0$ and further simplify the CRLB in (30) as

$$\mathrm{CRLB}(\varphi_{k,m}) \approx \left(\frac{\sigma_m}{a_k}\right)^2\frac{1}{2N}. \tag{31}$$

Sequentially, the CRLB of the Q-range for the RIPS-u is calculated from the CRLBs of $\varphi_{k,m}$ given in (31). According to (12), the Q-range is calculated by $\widehat{q}^{(u)} = \frac{c}{2\pi}\left(\frac{\widehat{\varphi}_{1,1}-\widehat{\varphi}_{1,2}}{f_1}-\frac{\widehat{\varphi}_{2,1}-\widehat{\varphi}_{2,2}}{f_2}\right)$. Hence, following the same transformation process as in the RIPS-sq, the CRLB of the Q-range for the RIPS-u is obtained from the CRLB of $\varphi_{k,m}$ as

$$\begin{aligned}\mathrm{CRLB}\left(q^{(u)}\right) &= \sum_{k=1}^{2}\sum_{m=1}^{2}\left(\frac{c}{2\pi f_k}\right)^2\mathrm{CRLB}(\varphi_{k,m}) \\ &= \left(\frac{c}{2\pi}\right)^2\frac{\sigma_1^2+\sigma_2^2}{2N}\left(\frac{1}{a_1^2f_1^2}+\frac{1}{a_2^2f_2^2}\right).\end{aligned} \tag{32}$$

The CRLB of the Q-range depends on $\sigma_m^2$, $a_k^2$, $N$, and $f_k$.

Now, let us investigate how different parameters affect the CRLBs in both systems. For simplicity, consider the special case where $\sigma_m^2 = \sigma^2$ and $a_1 = a_2 = a$. In such a case, the CRLB of the Q-range estimate with the RIPS-sq in (26) becomes

$$\gamma^{(\mathrm{sq})} = \left(\frac{c}{2\pi}\right)^2\frac{\sigma^2(\sigma^2+4a^2)}{a^4N}\left(\frac{1}{g^2}\right). \tag{33}$$

Similarly, the CRLB of the Q-range estimate with the RIPS-u in (32) becomes

$$\gamma^{(u)} = \left(\frac{c}{2\pi}\right)^2\frac{\sigma^2}{a^2N}\left(\frac{1}{f_1^2}+\frac{1}{f_2^2}\right). \tag{34}$$

Under this simplified scenario, the CRLBs of the Q-range estimates in both systems vs. signal-to-noise ratio (SNR) are plotted in Fig. 3. Here, we define the SNR at the $m$th receiver as $\left(a_1^2+a_2^2\right)/\left(\mathrm{PSD}_{v_m}\left(f_1\right)+\mathrm{PSD}_{v_m}\left(f_2\right)\right)$,

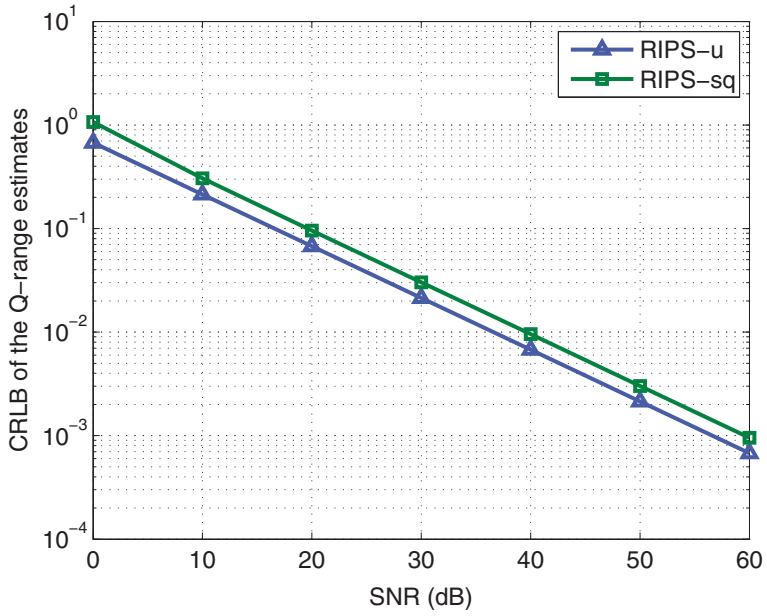


**Fig. 3** The CRLB of the Q-range estimates vs. SNR

where $\mathrm{PSD}_{v_m}(f)$ denotes a power spectral density of the noise $v_m(t)$ at frequency $f$. Since we model the noise as Gaussian distributed with variance $\sigma_m^2 = \sigma^2$ for $m = 1, 2$, $PSD_{v_m}(f_1) = \mathrm{PSD}_{v_m}(f_2) = \sigma^2$, and the SNR is $a^2/\sigma^2$. For illustration purposes here, we choose $g = 10$ MHz, $\Delta = 1.2$ kHz, $f_o = 9$ MHz, and $N = 100$. The CRLBs for both systems decrease with increasing SNR (a decreasing $\sigma^2$) as expected. Moreover, notice the 3-dB gap between two curves. This is because when $\sigma^2 \ll a^2$, the CRLB of the RIPS-sq in (33) is approximated as

$$\gamma^{(\mathrm{sq})} \approx \left(\frac{c}{2\pi}\right)^2 \frac{4\sigma^2}{a^2 N g^2}. \tag{35}$$

Also, assuming $\Delta \ll g$ such that $f_1 \approx f_2 \approx g$, (34) becomes

$$\gamma^{(u)} \approx \left(\frac{c}{2\pi}\right)^2 \frac{2\sigma^2}{a^2 N g^2} \approx 0.5\gamma^{(\mathrm{sq})}. \tag{36}$$

Hence, the RIPS-u achieves a 3-dB gain over the RIPS-sq.

When the SNR is fixed at 30 dB and $g$ is varied ($\Delta$ is fixed at 1.2 kHz), the CRLB also decreases as shown in Fig. 4. However, recall that frequencies affect the resolvable range. In other words, when the signals are transmitted at a higher frequency band, the performance improves at the cost of a reduction in the resolvable range. The effect of $\Delta$ on the CRLB with fixed $g$ is shown in Fig. 5. Both CRLB curves are flat since the CRLB of the RIPS-sq in (33) is independent of $\Delta$ and the change in $\Delta$ is small compared to $g$ for the RIPS-u in (34). Yet, a small $\Delta$ is desirable for the RIPS-sq since the approximated term $\eta$ depends on the the ratio $\Delta/g$. When $\Delta$ is large with respect to $g$, $\eta$ becomes a dominant source of error in the RIPS-sq.

Let us further analyze how signal amplitudes influence the performance. Constraining the total transmitting power as $a_1^2 + a_2^2 = 1$ and fixing the SNR at 30 dB, we plot the CRLB vs. $a_1^2$ in Fig. 6. The performance varies with different $a_1^2$, and the minimum CRLB is attained when $a_1^2 = a_2^2$ in both the RIPS-u and the RIPS-sq. Hence, equal transmitting power at two transmitters yields the best ranging performance in both systems.

### 4.3 The CRLB of the location estimates

Using the CRLBs for the Q-ranges derived in the previous subsections, the CRLBs of the location estimates in the RIPS-u and the RIPS-sq are derived. As we have described in Section 3, we assume that positions of three nodes are known at each ranging session. In the following derivations, since both systems require time synchronization between receivers, we fix the target node as the first transmitter. Considering a 2D scenario, we denote the coordinates of the target node and the $m$th receiver node as $\mathbf{x} = [x, y]^{\mathrm{T}}$ and $\mathbf{x}_m = [x_m, y_m]^{\mathrm{T}}$, respectively. Although we only consider a 2D scenario here, the same derivation can be applied for a 3D scenario. The Q-range can be represented as a function of $x$ and $y$ as

$$\begin{aligned} q = &\sqrt{(x - x_1)^2 + (y - y_1)^2} \\ &- \sqrt{(x - x_2)^2 + (y - y_2)^2} - d_{2,1} + d_{2,2}. \end{aligned} \tag{37}$$